Long nonlinear waves in resonance with topography

Jongho Choi and Paul A. Milewski*

April 19, 2002

Abstract

The evolution of periodic long surface waves over a periodic bottom topography resonant with the waves is studied. Coupled Korteweg-de Vries equations are derived and describe the evolution in terms of interaction between right- and left-travelling waves. The coupling arises from the cumulative effect of wave scattering. We discuss the various conserved quantities of the system and compute solutions for the initial value problem and for the time-periodic problem of fluid "sloshing" in a tank. Some three-dimensional extensions are discussed.

Keywords: Bragg resonance, topography, Korteweg–de Vries, sloshing

*address for correspondence: Department of Mathematics, University of Wisconsin-Madison, 480 Lincoln Dr., Madison, WI, 53706, e-mail: milewski@math.wisc.edu, tel: (608) 262–3220, fax: (608) 263–8891

1 Introduction

The interaction of gravity waves with physical inhomogeneities in the medium has been investigated in a variety of contexts by many researchers. A typical problem of this type is the scattering of surface waves by topography. The weak interaction of a field of gravity waves with an irregular bottom has been first analyzed theoretically by Hasselman [1] who provided the time rate of change of the wave spectrum as a linear functional of the spectrum of the bottom irregularity with coupling coefficients determined by the vertical eigenfunctions of the linear flat bottom problem. Long [2] used the theory to examine the case of surface waves propagating over an arbitrary spectrum of bottom perturbations in an attempt to explain swell decay observed in North Sea.

On natural beaches nearly periodic longshore sandbars can often be found. It is of particular interest in the field of sediment transport to understand the mechanism of wave-induced mass transport that forms offshore sandbars. It has been known that if there is enough reflection so that the waves are partially standing over an initially horizontal bottom, the Lagrangian drift near the boundary layer of the sea bottom can push heavy particles such as sand towards the nodes and light particles in suspension towards the antinodes, leading to the formation of sandbars on a seabed of wavelength one-half of the dominant incident waves. These periodic sandbars can in turn resonate strong reflected waves if the bar wavelength is one-half that of incident waves, which results in further development of sandbars offshore.

This kind of resonant reflection is well known as *Bragg reflection* in crystallography and has been central to a series of studies regarding surface wave reflection due to periodic topography. Davies and Heathershaw [3] considered the reflection of incident harmonic waves upon a patch of sinusoidal bottom ripples and compared the theory with laboratory observations in a wave tank. However the theory was limited to weak reflection and failed at resonance. Mei [4] derived the asymptotic equations uniformly valid in space and time which couple the slowly modulated incident and reflected wave envelopes through the bar amplitude, and provided a theoretically consistent prediction of significant reflection, although the theory did not describe the nonlinear effect.

The resonant interaction of two wave components with other periodic, steady components has been considered in broader geophysical contexts. Lelong and Riley [5] found that two travelling internal waves in stratified media exchange energy periodically with each other due to a steady potential vorticity, the mechanism of which is a resonant form of Bragg scattering. The problem where two irrotational surface wave modes interact resonantly with a third periodic, rotational, steady flow was studied by Milewski and Benney [6] considered the quartet resonant interaction between irrotational surface gravity waves with steady, vortical flows in the limit of deep water, and Milewski [7] studied the interaction in the limit of shallow water and derived two coupled Korteweg-de Vries equations and a streamfunction equation to describe the resonant interaction.

In this paper we consider the evolution of weakly nonlinear periodic surface waves over a periodic topography in the long wave limit. We are mainly concerned with the one-dimensional problem (the fluid domain is two-dimensional) and where the period of the topography is twice that of the waves (which is the case with the strongest interaction). This periodicity results in a triad interaction between the waves and the topography. Denoting by ω_1, ω_2 and k_1, k_2 the frequencies and the wave numbers of the surface wave modes, respectively, and by k_b the wave number of the bottom mode, the triad conditions for resonance are

$$\omega_1 + \omega_2 = 0,$$

$$k_1 + k_2 + k_b = 0.$$

Thus, $\omega_1 = -\omega_2$, $k_1 = k_2$, and $k_b = -2k_1$ and the bottom mode acts as a catalyst for the periodic energy exchange between two surface wave modes. The overall dynamics will be determined by the balance among this scattering mechanism, dispersion, and nonlinearity. Both the wave amplitudes and the bottom irregularity are taken to be small and of the same order. Over long time scales, the cumulative effect of the scattering couples the left- and right-propagating Korteweg-de Vries equations. The form of this coupling is a triad-like product in Fourier space which leads to a convolution in real space. Note that from its form, it is clear that the resonance we are considering is the spatial "dual" to subharmonic temporal resonances in the Faraday problem.

The remainder of this paper is organized as follows: In section 2 we derive the governing asymptotic equations. In section 3 the nature of the triad interaction described by the asymptotic equations are explained and three conservation laws are derived. In section 4 solutions of the linearized system is obtained. In section 5 numerical results for the time evolution of the equations are presented. In section 6, the traveling wave solutions are computed and the implication of the solutions as a wave motion in a confined wave tank is discussed. Finally, in section 7 we extend the framework to a three-dimensional situation where surface waves propagate obliquely over parallel topography.

2 Derivation of the asymptotic equations

Consider an irrotational flow of an incompressible inviscid fluid of uniform density with free surface $\hat{y} = h_0 + \hat{\eta}(x, z, t)$ and variable bottom $\hat{y} = \hat{b}(x, z)$, where h_0 is the average depth of the fluid. The dimensionless equations and boundary conditions governing the fluid motion are

$$\mu^2 \triangle\phi + \phi_{yy} = 0, \qquad \delta b < y < 1 + \epsilon\eta, \tag{2.1}$$

$$\phi_y = \delta\mu^2(b_x\phi_x + b_z\phi_z), \qquad y = \delta b, \tag{2.2}$$

$$\epsilon\eta_t + \epsilon\mu^2\nabla\eta\cdot\nabla\phi - \phi_y = 0, \qquad y = 1 + \epsilon\eta, \tag{2.3}$$

$$\epsilon\eta + \mu^2\phi_t + \frac{1}{2}\mu^2\phi_y^2 + \frac{1}{2}\mu^4|\nabla\phi|^2 = 0, \qquad y = 1 + \epsilon\eta. \tag{2.4}$$

where $\phi(x, y, z, t)$ is the velocity potential. The equations were nondimensionalized with

$$\hat{x} = lx, \quad \hat{z} = lz, \quad \hat{y} = h_0 y, \quad \hat{t} = \frac{l}{\sqrt{gh_0}}t, \quad \hat{\phi} = \frac{h_0^2\sqrt{gh_0}}{l}\phi, \quad \hat{\eta} = a\eta, \quad \hat{b} = \beta b,$$

where l denotes the characteristic wavelength. The two dimensionless wave parameters are $\epsilon = a/h_0, \mu^2 = (h_0/l)^2$, representing nonlinearity and dispersion respectively, and the topographic effect is measured by $\delta = \beta/h_0$. The operators $\triangle = \partial_x^2 + \partial_z^2$ and $\nabla = (\partial_x, \partial_z)$ apply only to horizontal coordinates.

As in the usual KdV limit, we set $\epsilon = O(\mu^2) \ll 1$. Assuming that δ is also small we expand the $\phi(x, y, z, t)$ and $\eta(x, z, t)$ in powers of ϵ and δ. From (2.1) and (2.2)

$$\begin{aligned} \phi(x, y, z, t) =& f(x, z, t) + \epsilon\left[-\frac{y^2}{2!}\triangle f\right] + \epsilon^2\left[\frac{y^4}{4!}\triangle^2 f\right] \\ &+ \epsilon\delta\left[y(b\triangle f + \nabla\cdot\nabla f)\right] + O(\epsilon^3, \delta^3, \cdots), \end{aligned} \tag{2.5}$$

where f is the leading order (depth independent) velocity potential. Solving (2.4) for η by using (2.5):

$$\begin{aligned} \eta(x, z, t) =& - f_t + \epsilon\left[\frac{1}{2}\triangle f_t - \frac{1}{2}|\nabla f|^2\right] \\ &+ \epsilon^2\left[-f_t\triangle f_t - \frac{1}{24}\triangle^2 f_t - \frac{1}{2}(\triangle f)^2 + \frac{1}{2}(f_x\triangle f_x + f_z\triangle f_z)\right] \\ &+ \epsilon\delta\left[-(b\triangle f_t + \nabla b\cdot\nabla f_t)\right] + O(\epsilon^3, \delta^3, \cdots). \end{aligned} \tag{2.6}$$

Finally, we obtain an evolution equation for $f(x, z, t)$ by substituting (2.6) and (2.5) in (2.3), and truncating the terms of $O(\epsilon^2, \delta^2, \epsilon\delta)$.

$$f_{tt} - h\triangle f = \epsilon\left[-\frac{1}{6}\triangle^2 f + \frac{1}{2}\triangle f_{tt} - f_t\triangle f - |\nabla f|_t^2\right] + \delta\left[-\nabla b\cdot\nabla f\right]. \tag{2.7}$$

Here, $h(x, z) = 1 - \delta b(x, z)$ is the local depth of the fluid. For $\delta = 0$, this is a Boussinesq-type equation known as the Benney-Luke equation [8]. We consider the case where the amplitude of the topography is comparable to that of the waves ($\epsilon = O(\delta)$).

For a one-dimensional free surface,

$$f_{tt} - hf_{xx} = \epsilon\left[-\frac{1}{6}f_{xxxx} + \frac{1}{2}f_{xxtt} - f_t f_{xx} - 2f_x f_{xt} - b_x f_x\right].$$

Since the linear speed of the waves $h^{1/2}$, an "optical length"

$$\tilde{x} = \int_{x_0}^{x} h^{-1/2}(s)\, ds$$

which makes the linear wave speed 1 is often introduced before further analysis. This is necessary for a number of cases of waves over slowly varying topography *compared* to the wavelength [9, 10, 11]. But since, in our case, fluctuations in wavespeed are small and of a period comparable to the wavelength,

$$\tilde{x} \sim (x - x_0) - \epsilon\frac{1}{2}\int_{x_0}^{x} b(s)\, ds,$$

this transformation is not necessary.

In the regime where topography varies on the scale of the waves, it is most important to describe the cumulative effect of reflections than to capture phase fluctuations which are stationary on average.

Substituting $h(x, z) = 1 - \delta b(x, z)$ into (2) we have

$$f_{tt} - f_{xx} = \epsilon\left[-\frac{1}{6}f_{xxxx} + \frac{1}{2}f_{xxtt} - f_t f_{xx} - (f_x^2)_t - (bf_x)_x\right]. \tag{2.8}$$

We split the solutions into left- and right- travelling waves with the power series expansions

$$f_t - f_x = u^{(0)} + \epsilon u^{(1)} + \cdots, \tag{2.9}$$

$$f_t + f_x = v^{(0)} + \epsilon v^{(1)} + \cdots, \tag{2.10}$$

where, using (2.6)

$$\eta = -\frac{1}{2}(u^{(0)} + v^{(0)}) + O(\epsilon).$$

Operating on (2.9) with $\partial_t + \partial_x$ and on (2.10) with $\partial_t - \partial_x$ we obtain

$$u_t^{(0)} + u_x^{(0)} = 0, \tag{2.11}$$

$$v_t^{(0)} - v_x^{(0)} = 0, \tag{2.12}$$

and

$$u_t^{(1)} + u_x^{(1)} = F(u^{(0)}, v^{(0)}, b), \tag{2.13}$$

$$v_t^{(1)} - v_x^{(1)} = F(u^{(0)}, v^{(0)}, b), \tag{2.14}$$

where the forcing term F is identical for both equations

$$\begin{aligned} F(u, v, b) = &-\frac{1}{6}u_{xxx} + \frac{1}{6}v_{xxx} + \frac{3}{4}uu_x - \frac{3}{4}vv_x \\ &+ \frac{1}{4}uv_x - \frac{1}{4}vu_x + \frac{1}{2}(bu)_x - \frac{1}{2}(bv)_x. \end{aligned}$$

We introduce the characteristic variables

$$\xi = x - t, \qquad \zeta = x + t, \tag{2.15}$$

and proceed with the method developed in [7] to modify the leading order equations (2.11,2.12) in order to remove secularities in next order terms $u^{(1)}, v^{(1)}$ in (2.9, 2.10). The main step, for (2.13) is to write

$F(u^{(0)}, v^{(0)}, b)(\xi, t) = \bar{F}(\xi) + \tilde{F}(\xi, t)$, that is, to write F as the sum of an average and fluctuation in a frame moving with the linear wave speed. The time independent average $\bar{F}$ is the component that gives rise to secular behavior in (2.13), and is used to modify the leading order equation (2.11) for $u^{(0)}$. For equation (2.14) the process is repeated with the independent variables ζ and t. Thus we modify (2.11) to

$$u_t^{(0)} + u_x^{(0)} = \epsilon \bar{F}, \tag{2.16}$$

where, assuming that the bottom and the two waves have zero mean and that they are periodic in their respective variables with period $2L$,

$$\bar{F} = -\frac{1}{6}u_{xxx}^{(0)} + \frac{3}{4}u^{(0)}u_x^{(0)} - \frac{1}{2}\left(\frac{1}{2L}\int_{-L}^{L}\left[b(\xi+t)v^{(0)}(\xi+2t)\right]_\xi dt\right).$$

After integrating by parts the last term and repeating the procedure for the left-travelling wave we obtain

$$u_t^{(0)} + u_x^{(0)} = \epsilon\left[-\frac{1}{6}u_{xxx}^{(0)} + \frac{3}{4}u^{(0)}u_x^{(0)} + \frac{1}{2}\left\langle bv_x^{(0)}\right\rangle\right], \tag{2.17}$$

$$v_t^{(0)} - v_x^{(0)} = \epsilon\left[\frac{1}{6}v_{xxx}^{(0)} - \frac{3}{4}v^{(0)}v_x^{(0)} - \frac{1}{2}\left\langle bu_x^{(0)}\right\rangle\right], \tag{2.18}$$

where

$$\left\langle bv_x^{(0)}\right\rangle = \frac{1}{2L}\int_{-L}^{L} b(\xi+t)v_\xi^{(0)}(\xi+2t)\,dt,$$

$$\left\langle bu_x^{(0)}\right\rangle = \frac{1}{2L}\int_{-L}^{L} b(\zeta-t)u_\zeta^{(0)}(\zeta-2t)\,dt.$$

The terms on the right-hand side are the familiar KdV dispersive and nonlinear terns, and, interaction terms representing the cumulative effect of reflections on the topography. The convolution integrals can be interpreted as summing all the contributions from triads $k_1 + k_2 + k_b/2 = 0$ over the Fourier spectra of the waves, as we will show below.

We introduce the slow (KdV) time scale $\tau = \epsilon t$ and rescale the equations with:

$$u(\xi,\tau) = -u^{(0)}, \qquad v(\zeta,\tau) = -v^{(0)}, \qquad b = \frac{3}{2}\tilde{b}, \qquad (\xi,\zeta) = \sqrt{\frac{2}{9}}(\tilde{\xi},\tilde{\zeta}), \qquad \tau = \sqrt{\frac{32}{81}}\tilde{\tau}$$

then after dropping tildes, (2.17) and (2.18) become

$$u_\tau + uu_\xi + u_{\xi\xi\xi} = \langle bv_\zeta\rangle, \tag{2.19}$$

$$v_\tau - vv_\zeta - v_{\zeta\zeta\zeta} = -\langle bu_\xi\rangle. \tag{2.20}$$

The leading terms of surface elevation and horizontal fluid velocity can be recovered by

$$\eta^{(0)} = \frac{1}{2}(u+v), \qquad f_x^{(0)} = \frac{1}{2}(u-v).$$

In subsequent sections we use equations (2.19), (2.20) for simplicity and easy comparison with classical results on the unidirectional KdV equation

$$u_\tau + uu_\xi + u_{\xi\xi\xi} = 0. \tag{2.21}$$

3 Properties and conserved quantities of the equations

Let 2L be the smallest common period of u, v, b. We can then write u, v as Fourier series

$$u(\xi,\tau) = \sum_{m=-\infty}^{\infty}\hat{u}_m(\tau)e^{ik_m\xi}, \qquad v(\zeta,\tau) = \sum_{m=-\infty}^{\infty}\hat{v}_m(\tau)e^{ik_m\zeta}, \tag{3.22}$$

where

$$k_m = \frac{\pi}{L} m, \qquad \hat{u}_m^* = \hat{u}_{-m}, \qquad \hat{v}_m^* = \hat{v}_{-m},$$

and * denotes complex conjugate. Then, for a sinusoidal bottom

$$b(x) = Be^{ik_b x} + B^* e^{-ik_b x},$$

(2.19),(2.20) become

$$u_\tau + uu_\xi + u_{\xi\xi\xi} = ik_M \left[B^* \hat{v}_M(\tau) e^{-ik_M \xi} - B \hat{v}_M^*(\tau) e^{ik_M \xi} \right], \tag{3.23}$$

$$v_\tau - vv_\zeta - v_{\zeta\zeta\zeta} = -ik_M \left[B^* \hat{u}_M(\tau) e^{-ik_M \zeta} - B \hat{u}_M^*(\tau) e^{ik_M \zeta} \right], \tag{3.24}$$

where M is defined such that $k_M = \frac{k_b}{2}$. Therefore, the components of u and v with wavenumber $\pm\frac{k_b}{2}$ are the only ones that interact, by forming a resonant triad with the single bottom mode of wavenumber $\mp k_b$. The other Fourier modes do not feel the bottom directly, although they do so indirectly through the nonlinear terms. We note that the form of each equation in (3.23) and (3.24) is of KdV forced by a sinusoid of fixed period (as in [12]) but whose amplitude and phase vary with time (since it depends on the amplitude of a Fourier mode of the other equation).

When the topography consists of multiple Fourier modes, the interaction terms in the equations must sum over all possible triads. (The convolution in physical space is the sum of products in Fourier space.) Thus, for a general periodic topography

$$b(x) = \sum_{l=-\infty}^{\infty} \hat{b}_l e^{ik_l x}, \qquad k_l = \frac{\pi}{L} l, \qquad \hat{b}_l^* = \hat{b}_{-l},$$

the topographical coupling terms become

$$\langle bv_\zeta \rangle = \sum_{l=-\infty}^{\infty} (-ik_{M_l})\, \hat{b}_l \hat{v}_{M_l}^*(\tau) e^{ik_{M_l}\xi}, \qquad \langle bu_\xi \rangle = \sum_{l=-\infty}^{\infty} (-ik_{M_l})\, \hat{b}_l \hat{u}_{M_l}^*(\tau) e^{ik_{M_l}\zeta},$$

where M_l is such that $k_{M_l} = \frac{k_l}{2}$. These sums are the cumulative effects of the multiple triads due to multiple topographic modes.

The system of equations (2.19), (2.20) possess at least three invariants which correspond to conservations of mass, momentum, and energy:

$$I_1 = I_{1u} + I_{1v} = \int_{-L}^{L} u \, d\xi + \int_{-L}^{L} v \, d\zeta, \tag{3.25}$$

$$I_2 = \int_{-L}^{L} \frac{1}{2} u^2 \, d\xi + \int_{-L}^{L} \frac{1}{2} v^2 \, d\zeta, \tag{3.26}$$

$$I_3 = \int_{-L}^{L} \left(\frac{1}{3} u^3 - u_\xi^2 \right) d\xi + \int_{-L}^{L} \left(\frac{1}{3} v^3 - v_\zeta^2 \right) d\zeta + 2 \int_{-L}^{L} \langle uv \rangle \, b \, dx, \tag{3.27}$$

where

$$\langle uv \rangle (x, \tau) = \frac{1}{2L} \int_{-L}^{L} u(x - t, \tau) v(x + t, \tau) \, dt. \tag{3.28}$$

Derivations of these invariant quantities are given in the Appendix. Clearly, they correspond to the first 3 conserved quantities of the KdV equation if there is no topography. In terms of Fourier coefficients, the nonlocal term in I_3 is

$$2 \int_{-L}^{L} \langle uv \rangle \, b \, dx = 4L \sum_{m=-\infty}^{\infty} \hat{u}_m(\tau) \hat{v}_m(\tau) \hat{b}_{2m}^*,$$

which shows again the resonant triad $k_1 + k_2 + k_b = 0$ with $k_1 = k_2 = -k_b/2$. These conserved quantities are used to monitor our numerical computations. Notice that in (3.25) each integral is also an invariant.

Defining the functional H by

$$H\{u,v\} = -\frac{1}{2}I_3.$$

then (2.19), (2.20) can be written in the Hamiltonian form

$$\frac{\partial}{\partial\tau}\begin{pmatrix} u \\ v \end{pmatrix} = D\begin{pmatrix} \delta H/\delta u \\ \delta H/\delta v \end{pmatrix},$$

where D is the following operator,

$$D = \begin{pmatrix} \frac{\partial}{\partial\xi} & 0 \\ 0 & -\frac{\partial}{\partial\zeta} \end{pmatrix}.$$

Here $\delta H/\delta u, \delta H/\delta v$ mean the functional derivatives of H with respect to u, v respectively.

Furthermore, introducing the potentials

$$u = \Phi_\xi, \qquad v = \Psi_\zeta$$

and define the Lagrangian by

$$\begin{aligned}
\mathcal{L} &= \int_{-L}^{L} \Phi_\tau \frac{\delta\mathcal{L}}{\delta\Phi_\tau}\, d\xi - \int_{-L}^{L} \Psi_\tau \frac{\delta\mathcal{L}}{\delta\Psi_\tau}\, d\zeta - H \\
&= \int_{-L}^{L} \left(\frac{1}{2}\Phi_\xi\Phi_\tau + \frac{1}{6}\Phi_\xi^3 - \frac{1}{2}\Phi_{\xi\xi}^2\right) d\xi + \int_{-L}^{L} \left(-\frac{1}{2}\Phi_\zeta\Phi_\tau + \frac{1}{6}\Phi_\zeta^3 - \frac{1}{2}\Phi_{\zeta\zeta}^2\right) d\zeta \\
&+ \int_{-L}^{L} \langle uv\rangle\, b\, dx,
\end{aligned}$$

the equations (2.19), (2.20) can also be obtained from the variational (Hamilton's least action) principle

$$\delta \int \mathcal{L}\, d\tau = 0.$$

4 Solutions of the linearized system

We now consider solutions to the linearized equations

$$u_\tau + u_{\xi\xi\xi} = \langle bv_\zeta\rangle, \tag{4.29}$$
$$v_\tau - v_{\zeta\zeta\zeta} = -\langle bu_\xi\rangle. \tag{4.30}$$

These can be obtained from the physical problem if the wave amplitudes are small compared to the topography and dispersive effects ($\mu^2 = \delta \gg \epsilon$). We seek solutions to (4.29), (4.30) of the form

$$\begin{aligned}
u &= A_u e^{i(k\xi - \omega_u\tau)} + *, \\
v &= A_v e^{i(k\zeta - \omega_v\tau)} + *,
\end{aligned}$$

where $b(x) = Be^{ik_b x} + *$ and $k = -k_b/2$. Substitution into (4.29), (4.30) yields the linear dispersion relations

$$\omega_u^\pm = -k^3 \pm |kB|, \tag{4.31}$$
$$\omega_v^\pm = k^3 \mp |kB|, \tag{4.32}$$

with solutions written

$$u(\xi,\tau) = |kB|Ce^{i(k\xi-\omega_u^+\tau)} + |kB|De^{i(k\xi-\omega_u^-\tau)} + *, \tag{4.33}$$
$$v(\zeta,\tau) = kB^*C^*e^{i(k\zeta-\omega_v^+\tau)} - kB^*D^*e^{i(k\zeta-\omega_v^-\tau)} + *. \tag{4.34}$$

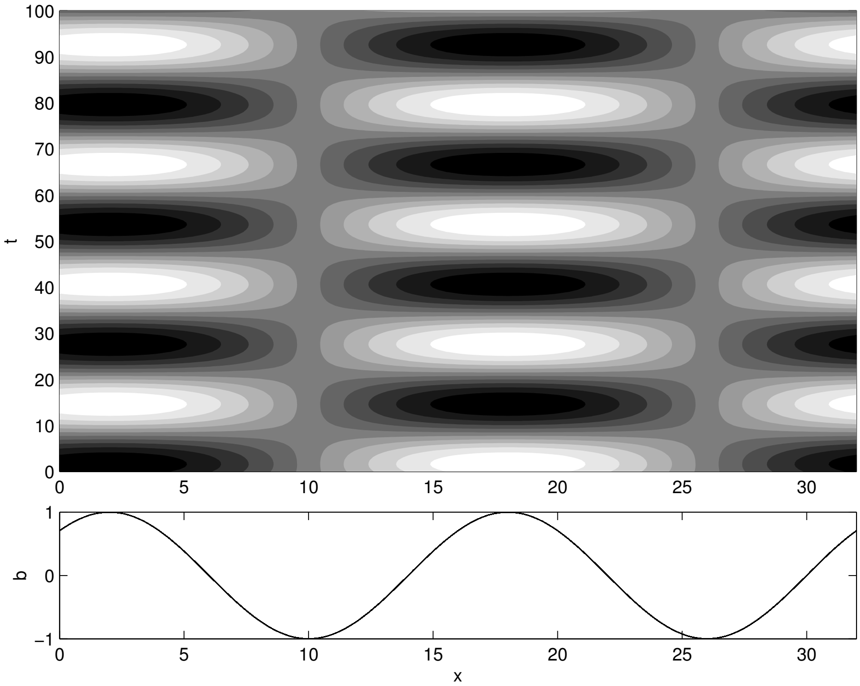

Figure 1: Free surface elevation (crests are darker) from (4.33,4.34) and the underlying topography. The figure was drawn with $D = 0$, $\epsilon = 0.5$, $C = 1$, $B = (1 + i)/\sqrt{8}$.

For a more general periodic topography, these dispersion relations apply for all modes k such that there is a Fourier component of the bottom with $k_b = -2k$, and then $B = \hat{b}(k_b) = \hat{b}(-2k)$. Modes which do not resonate with the bottom satisfy the uncoupled system and have $\omega_u = -k^3$ and $\omega_v = k^3$. General solutions to (4.29), (4.30) can be obtained by superposition.

We can understand these solutions by considering the case $D = 0$ in (4.33,4.34). This solution is composed of two sinusoidal modes of equal amplitude travelling at speeds (for $k > 0$)

$$1 - \epsilon\frac{1}{6}k^2 + \epsilon\frac{1}{2}|B|, \qquad -1 + \epsilon\frac{1}{6}k^2 - \frac{1}{2}\epsilon|B|$$

in the original dimensionless variables of (2). This yields a standing wave with nodes on the *troughs* of the topography (see Figure 1).

Note that since the speed is *increased* from the case $B = 0$, the period of the standing wave is *decreased* from a similar standing wave which can be constructed when there is no topography. Similarly, taking $C = 0$ yields, for $k > 0$ a standing wave with nodes on the *crests* of the topography with a period that is *increased* by the topography.

When these two motions are superposed, the wave motion is periodic or quasiperiodic in time. Figure 2 shows an example of this.

5 Numerical solutions

Numerical solutions of (2.19), (2.20) have been computed for various cases by an integrating factor method [13] combined with a Runge-Kutta scheme for the time evolution. Since the method consists of directly computing the evolution of the Fourier coefficients of the solution, the nonlocal convolution terms are easily computed as products. The computations shown were obtained with 256 Fourier modes. However, in most cases 64 modes are sufficient.

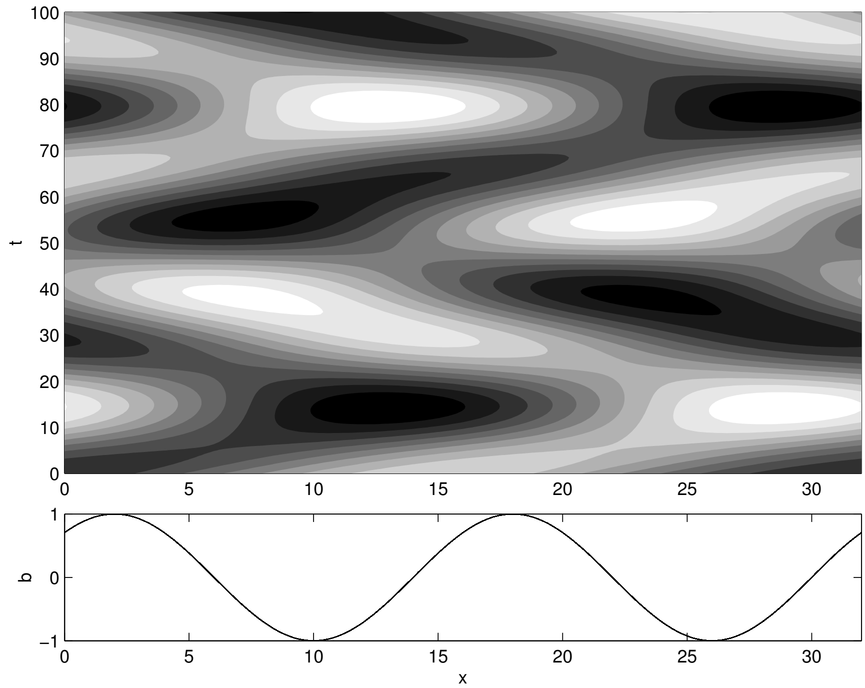

Figure 2: Free surface elevation (crests are darker) from (4.33,4.34) and the underlying topography. The figure was drawn with $\epsilon = 0.5$, $C = 1$, $D = 1.5$, $B = (1+i)/\sqrt{8}$.

In the following set of experiments, the computational domain is $[0, 32]$ and the bottom is given by

$$b(x) = B\cos\left(\frac{\pi}{8}x\right),$$

which has the period one half of the longest mode on the domain to clearly demonstrate the resonant effect. There are three effects in the system (2.19), (2.20): wave steepening nonlinearity, dispersion, and scattering. The nonlinearity and dispersion together combine to allow the propagation of solitons in KdV. The scattering tends to reflect portions of the spectra of the waves. Thus, if the scattering (parametrized by B) is small compared to the amplitude of the initial data, one expects solutions which can be understood by considering a perturbation of a KdV solution.

An example of this is shown in Figure 3, 4 where the initial data consists of a solitary wave (repeated periodically) for the right-travelling mode u and zero for the left-travelling mode v, and the topography is small. Figure 3 shows the solutions in the KdV variables (note that the amplitude of v remains small) and Figure 4 shows the reconstruction of the free surface in the physical variables. This shows clearly that the solution is mostly composed of right-propagating solitons together with a weak reflected travelling-standing component. Figure 5, 6 show the solutions for the same initial data and larger topography. Here, it is clear from Figure 5 that there is large exchanges between right- and left- travelling waves, and that, furthermore this exchange happens slowly enough for there to be coherent propagation in each direction. From the reconstructed solution in 6, the original right-propagating waves survive until $t \approx 100$, after which most energy is in the left-propagating wave. This behavior appears to repeat periodically. Figure 7, 8, show the result of increasing further the topography. Here, the topography exchanges energy more rapidly between the two modes (note that ω increases with B in 4.31,4.32) and this short time scale prevents the nolinearity from acting in a coherent manner.

One can summarize these results with Figure 9 which shows the total energy in the right- and left- travelling mode. Note that for B small the energy remains in the initial mode, for intermediate B there is a periodic exchange of energy, and that for B larger the solution involves more complicated energy transfer.

Typical solutions for more general initial data (initial data that are not travelling waves of KdV) are shown in Figures 10–13. Figures 10, 11 show the solution where the initial data for the right-travelling wave

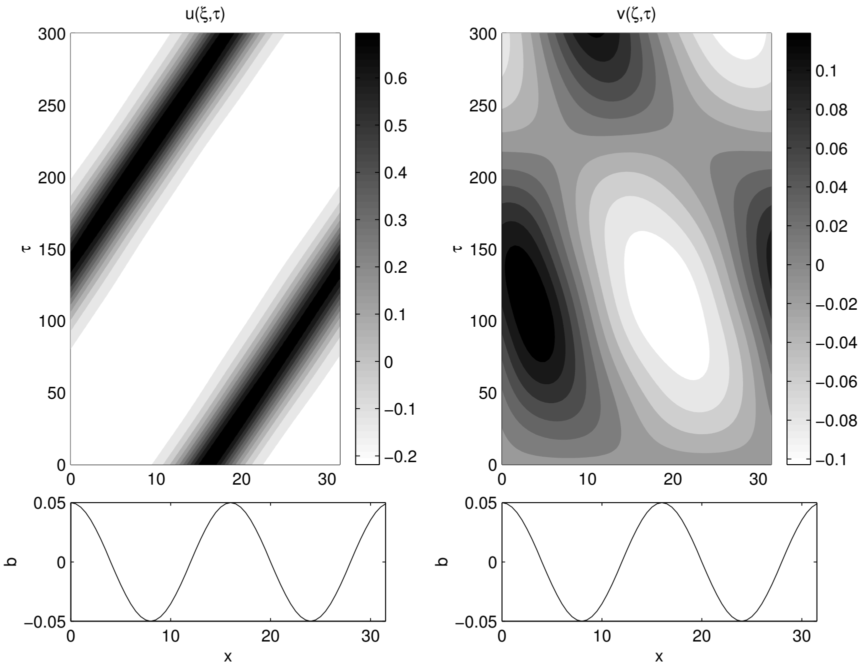

Figure 3: Solutions of (3.23), (3.24) with $b = 0.05\cos(\frac{\pi}{8}x)$ and initial conditions $u = \operatorname{sech}^2\left(\frac{1}{\sqrt{12}}(x-16)\right)$, $v = 0$.

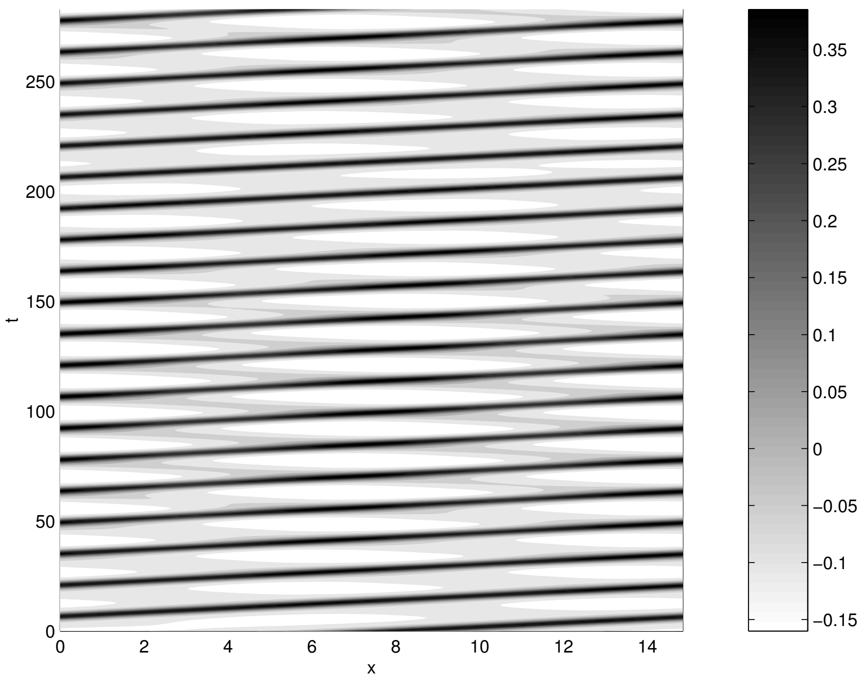

Figure 4: Free surface elevation corresponding to Figure 3.

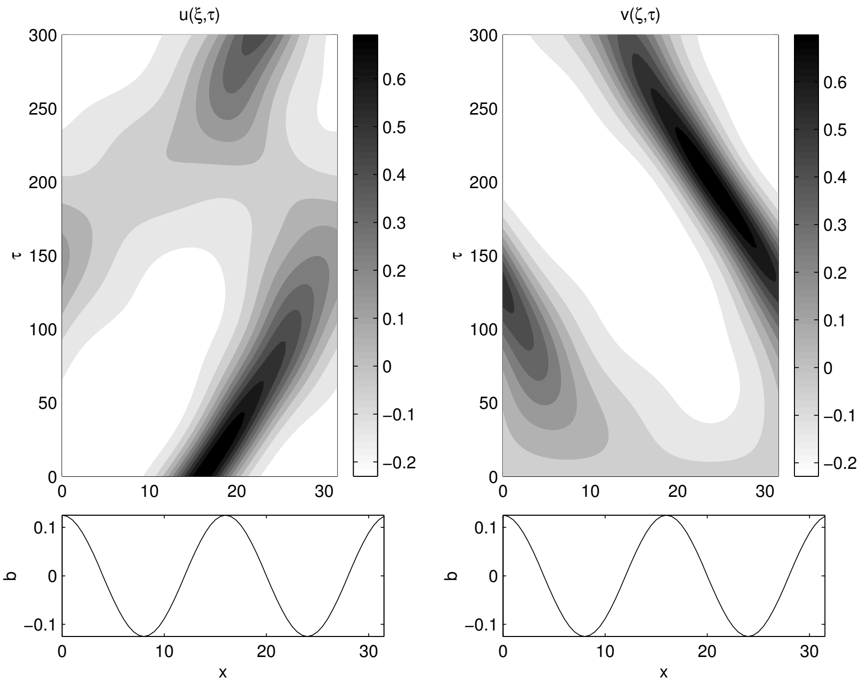

Figure 5: Solutions of (3.23), (3.24) with $b = 0.125\cos(\frac{\pi}{8}x)$ and initial conditions $u = \mathrm{sech}^2\left(\frac{1}{\sqrt{12}}(x-16)\right)$, $v = 0$.

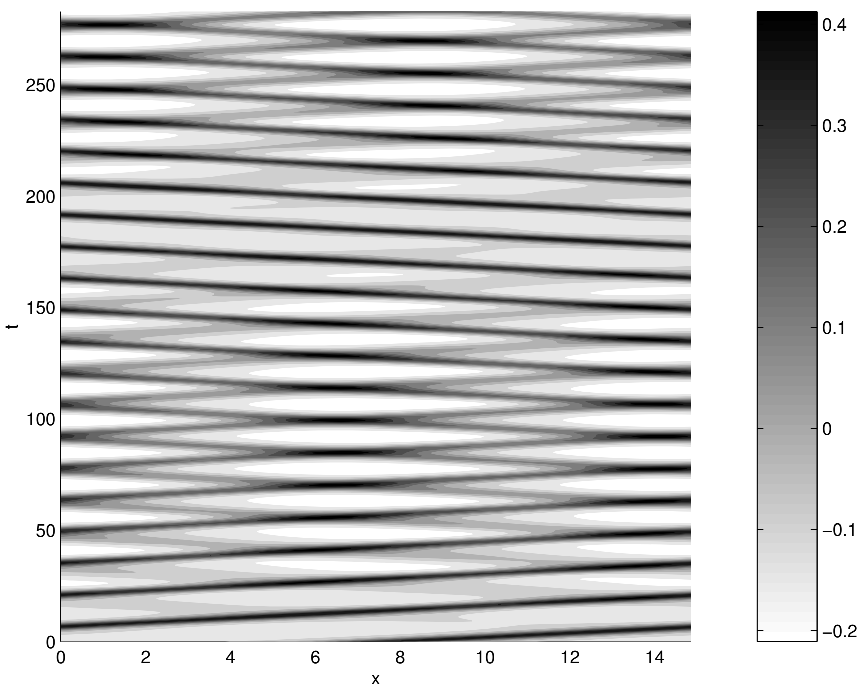

Figure 6: Free surface elevation corresponding to Figure 5.

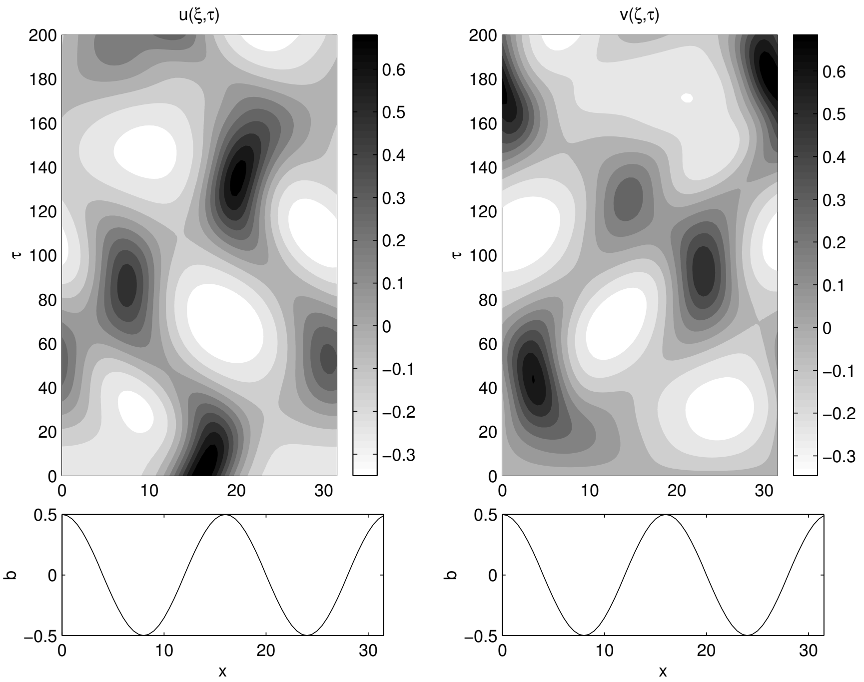

Figure 7: Solutions of (3.23), (3.24) with $b = 0.5\cos(\frac{\pi}{8}x)$ and initial conditions $u = \mathrm{sech}^2\left(\frac{1}{\sqrt{12}}(x-16)\right)$, $v = 0$.

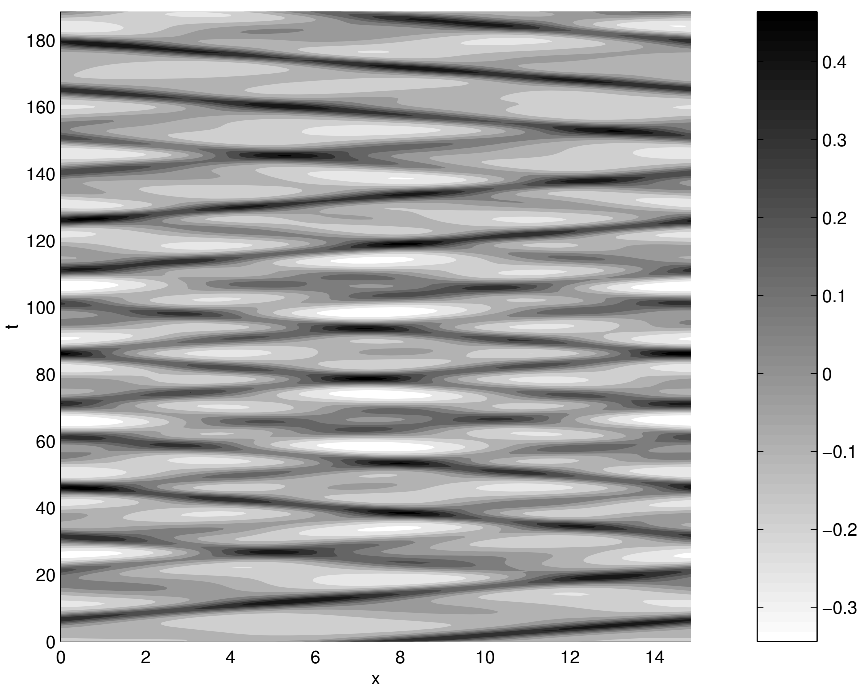

Figure 8: Free surface elevation corresponding to Figure 7.

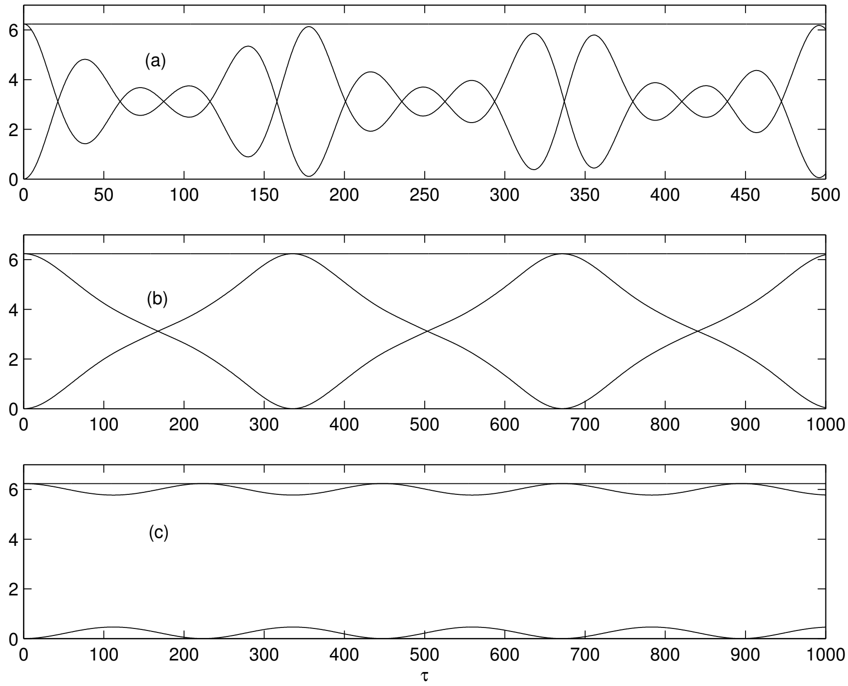

Figure 9: Energy of solutions of (3.23), (3.24) with $b = B\cos(\frac{\pi}{8}x)$ and initial conditions $u = \operatorname{sech}^2\left(\frac{1}{\sqrt{12}}(x-16)\right)$, $v = 0$. In (a), $B = 0.5$, in (b) $B = 0.1$, in (c), $B = 0.05$.

is a sinusoid, the initial data for the left-travelling wave is zero, and there is no topography. The solution consists of the breaking up of the initial data into three waves (see Figure 11 for $0 < t < 10$) which then undergo several repeated interactions due to the periodicity of the problem. Obviously v remains zero. As the topography increases there is now energy exchange between the modes. In Figure 12 we clearly see a coherent left-travelling wave generated.

6 Time periodic solutions and sloshing motion

A particular physical situation where the type of wave-topographical interaction is important is the "sloshing" of a shallow fluid in a container of size $2L$ with an undulating bottom of period L. To satisfy the boundary condition of zero horizontal velocity at the walls, we need to impose (using 2) that $u = v$ at $x = \pm L$.

One method to find time-periodic solutions in such a situation is to seek "travelling" wave solutions of (3.23), (3.24) by writing

$$u = g(\theta), \qquad \theta = \xi - C\tau,$$
$$v = h(\phi), \qquad \phi = \zeta + C\tau.$$

Since these modes are travelling at speed $\pm(1+\epsilon C)$ and they they are periodic in space, they will also be periodic in time with period $2L/(1+\epsilon C)$.

Substituting into (3.23), (3.24), we have

$$-Cg_\theta + gg_\theta + g_{\theta\theta\theta} = ik_M\left[B^*\hat{h}_M e^{-ik_M\theta} - *\right], \tag{6.35}$$

$$-Ch_\phi + hh_\phi + h_{\phi\phi\phi} = ik_M\left[B^*\hat{g}_M e^{-ik_M\phi} - *\right]. \tag{6.36}$$

Notice that these two equations are the same. In order to satisfy the boundary conditions at the walls, we choose (without loss of generality) $g = h$, and that they are even functions about 0. (This choice imposes

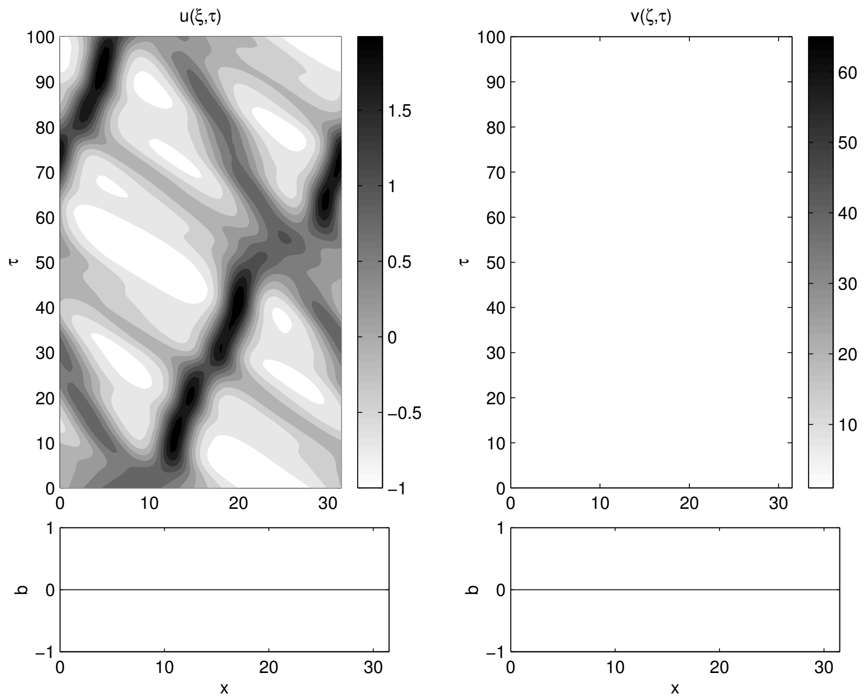

Figure 10: Solutions of (3.23), (3.24) with $b = 0$ and initial conditions $u = \sin\left(\frac{\pi}{16}x\right)$, $v = 0$.

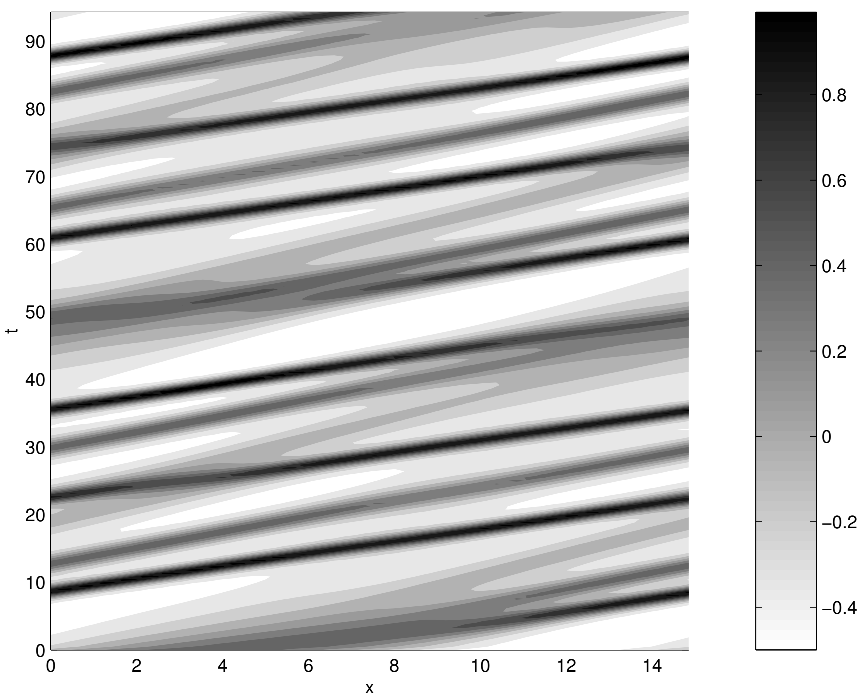

Figure 11: Free surface elevation corresponding to Figure 10.

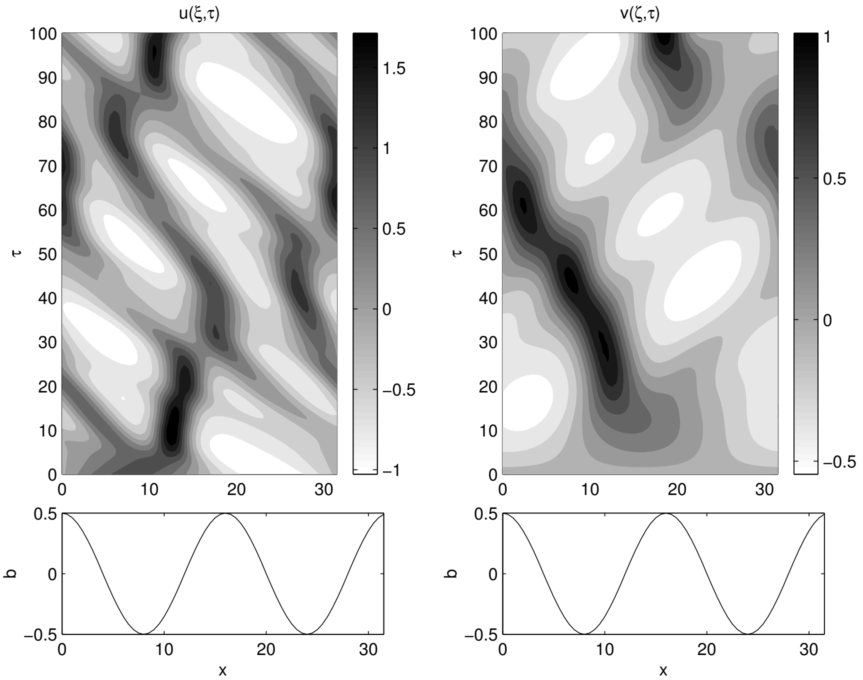

Figure 12: Solutions of (3.23), (3.24) with $b = 0.5\cos(\frac{\pi}{8}x)$ and initial conditions $u = \sin\left(\frac{\pi}{16}x\right)$, $v = 0$.

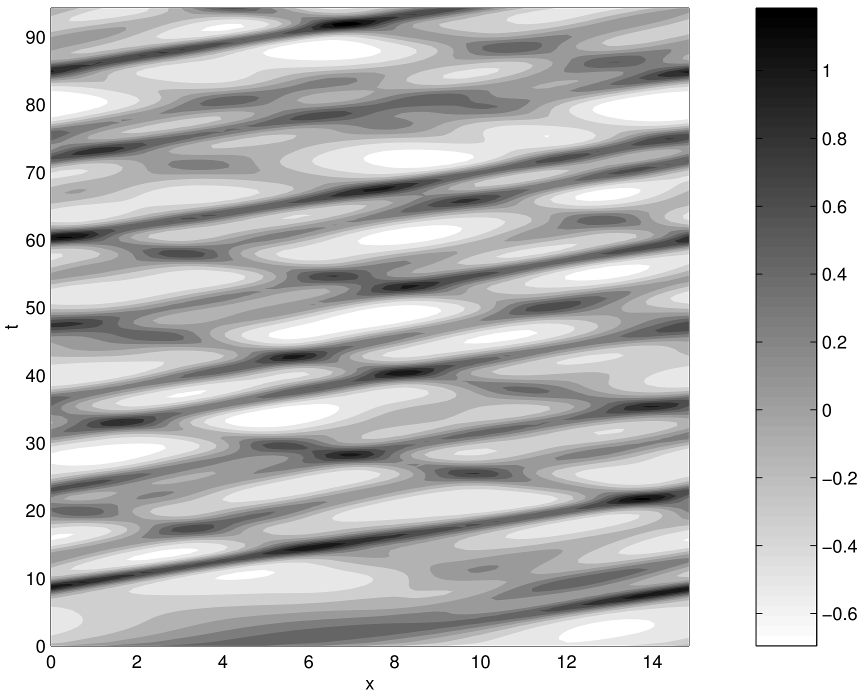

Figure 13: Free surface elevation corresponding to Figure 12.

that u and v are images of each other about $x = \pm L$ and that, therefore $u - v$ is zero there.) Clearly, in the full time-dependent case there may be asymmetric sloshing solutions where u, v are not images of each other.

Integrating the resulting equation once, one obtains

$$-Cg + \frac{1}{2}g^2 + g_{\theta\theta} \;\; = - \left[B^* \hat{g}_M e^{-ik_M\theta} + *\right] + A, \tag{6.37}$$

Since we impose that the average of g is zero, $A = \frac{1}{2}\int_{-L}^{L} g^2 d\theta$ is the energy of the wave. Since g is even, the left-hand side of (6.37) is even and therefore the right-hand side must also be even. Thus solutions are only possible with even topography. In our simplest case we choose a single cosine $b(x) = \beta \cos k_b x$ so that $B = B^* = \frac{1}{2}\beta$. Then, (6.37) becomes

$$-Cg + \frac{1}{2}g^2 + g_{\theta\theta} \;\; = -\beta \hat{g}_M \cos(k_M\theta) + A, \tag{6.38}$$

where $k_M = \pi/L$.

Solutions of (6.38) have been approximated numerically by using Newton's method on the finite set of nonlinear algebraic equations resulting from truncating the Fourier cosine series for g. Suppose that the computing domain is given by $[-L, L]$. Look for the truncated Fourier series solutions of the form

$$\mathbf{g}(\theta) = \sum_{n=-N}^{N} a_n e^{in\frac{\pi}{L}\theta}, \tag{6.39}$$

where $a_n = a_{-n}$ are real. We substitute (6.39) into (6.38) and impose $a_0 = 0$ to obtain a real solution with zero average. Fixing $\sum_{n=1}^{N} a_n^2$ which is, by Parceval's equality, equivalent to fixing the energy of the solution, we obtain a system of $N + 1$ nonlinear algebraic equations for $N + 1$ unknowns $a_1, \ldots, a_N$ and phase speed C. Generally, branches of solutions are easy to find, either by starting with known KdV solutions for $\beta = 0$ and following the solution branch by continuation in β, or by starting with the linear solution (4.33) for fixed β and continuing the solution in A (the energy of the solution).

A diagram of the branches of solutions is shown in Figure 14. The diagram was obtained with $L = 16$ and 128 cosine modes. In this figure the bold curves are various branches of solutions at *fixed* energy showing the dependence of the speed c on the topography amplitude β. The dashed diagonal line is the speed of the linear standing wave in (4.33) that has zero horizontal velocity at $x = \pm L$. The horizontal lines denote periodic (cnoidal) solutions of KdV with period $2L/m$ for $m = 2, 3, 4$. Since these cnoidal waves have Fourier coefficient equal to zero for $k_M = \pi/L$, they are also solutions to (6.38) independent of β. The point denoted with a circle is the solution to KdV with period $2L$. The labels (i)-(v) correspond to points on the curve for which solutions are shown in Figures 15-17.

Figure 15 shows a cnoidal solution to KdV (i) together with a typical solution for $\beta > 0$ on the upper branch (ii). We note that the solutions here travel *faster* than the solitary wave although they are less steep. In fact, as β increases, solutions along this branch tend to a *finite amplitude* cosine standing wave with nodes on the troughs of the topography. In this limit, although nonlinearity is present, the rapid oscillations of the free surface prevent them from having a strong effect. Figure 16 shows a typical solution for $\beta < 0$ on the upper branch (iii), together with the cnoidal solutions to KdV with period $2L$ (i) and with period L ($m = 2$). This typical solution, for sufficiently negative β has 2 crests and tends to the cnoidal $m = 2$ solution which is not, in this limit, affected by the bottom. (Recall that the interaction we consider here is the cumulative effect of many passages over the topography, and for waves with zero Fourier component of period $2L$, this cumulative effect averages to zero in the limit we are considering.)

Figure 17 shows typical solutions on the second branch of figure 14. This branch appears to be a nonlinear connection between the $m = 2$ and the $m = 3$ cnoidal solutions. Indeed, at (iv) the solutions have two crests and as one approaches (v) the solutions develop an additional crest. Lower branches shown in figure 14 are similar, connecting solutions with m crests to $m + 1$ crests. Lastly, figure 18 shows the reconstruction of the free-surface evolution for the case (iii) discussed above.

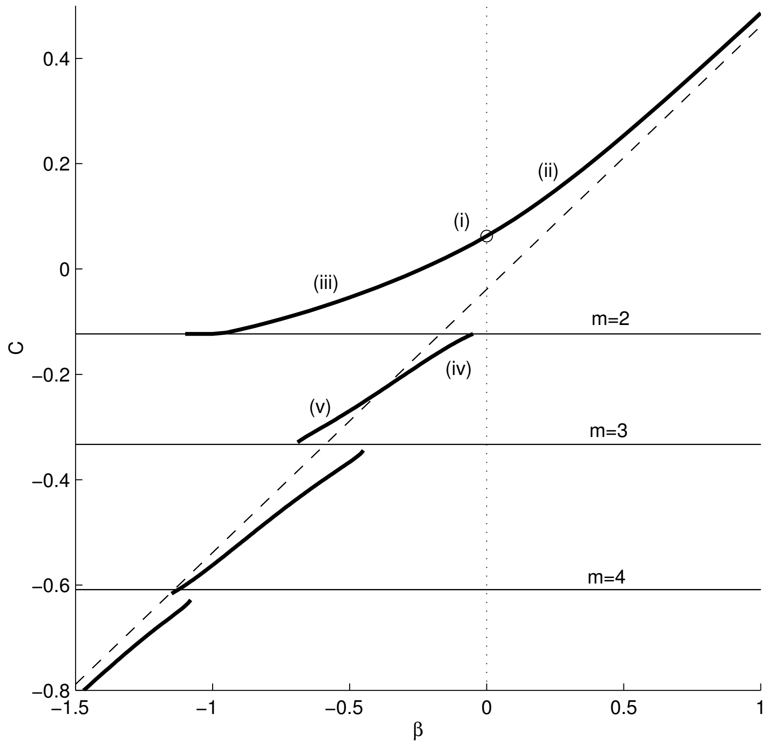

Figure 14: Branches of solutions for (6.38) with mean zero and $A = 0.9383$.

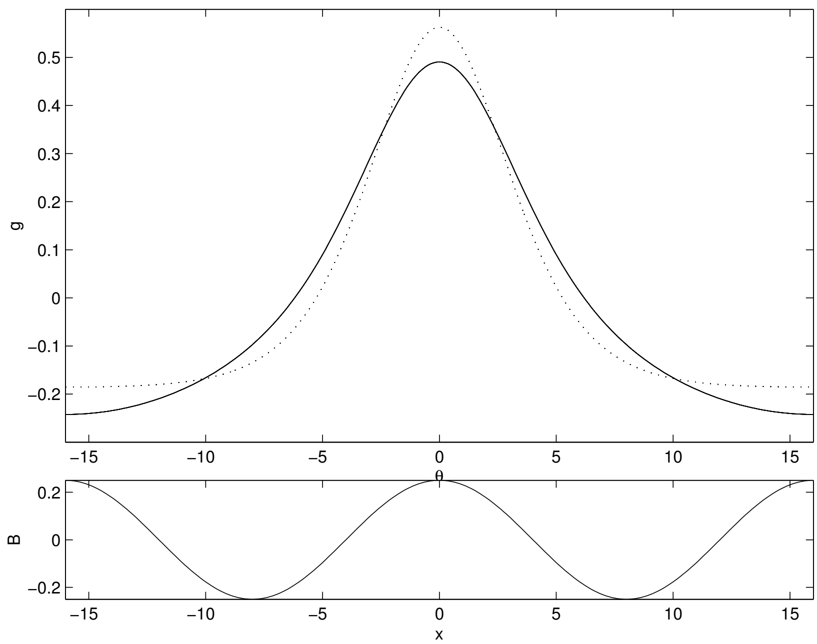

Figure 15: Solutions of (6.38) at (i) and (ii) in Figure 14. (i) Dotted curve: $\beta = 0$, and $C = 0.0626$. (ii) Solid curve: $\beta = 0.25$ and $C = 0.1490$. The topography is shown for (ii).

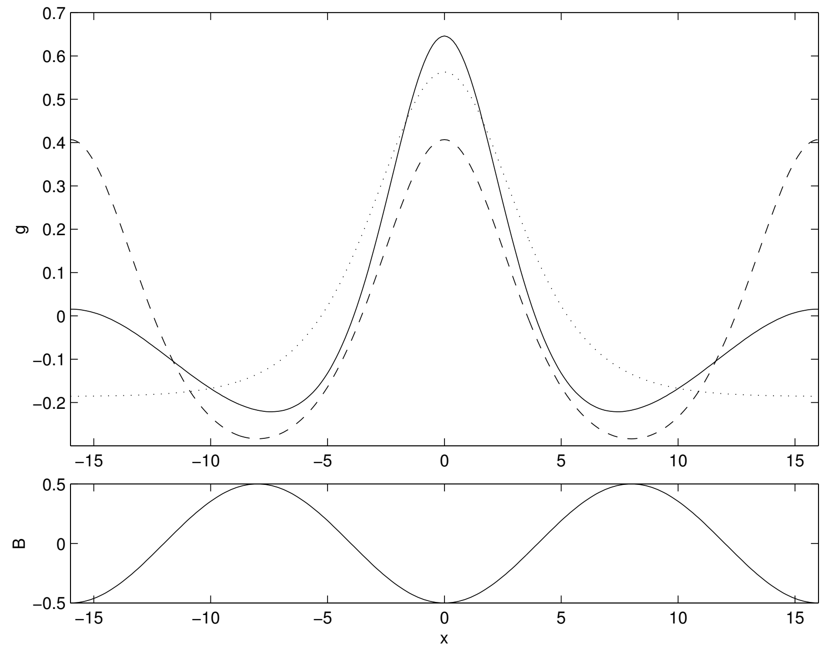

Figure 16: Solutions of (6.38) at (i),(iii) and of the $m = 2$ cnoidal wave in Figure 14. (i) Dotted curve: $\beta = 0$, and $C = 0.0626$. (iii) Solid curve: $\beta = -0.5$ and $C = -0.0540$. Dashed curve: $m = 2$ cnoidal wave, $C = -0.1233$, solution is independent of β. The topography is shown for (iii).

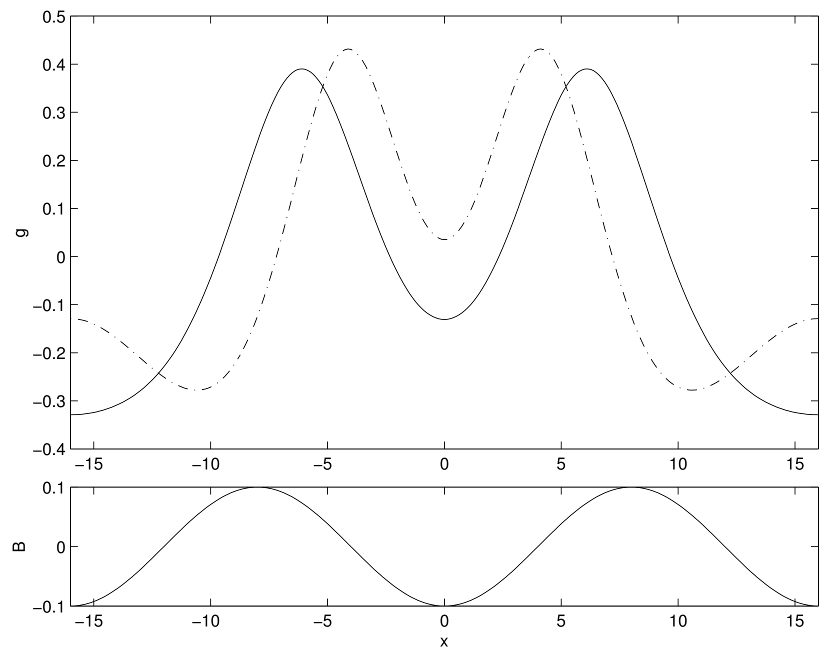

Figure 17: Solutions of (6.38) at (iv),(v) in Figure 14. (iv) Solid curve: $\beta = -0.1$, and $C = -0.1359$. (v) Dash-dot curve: $\beta = -0.65$ and $C = -0.3157$. The topography is shown for (iv).

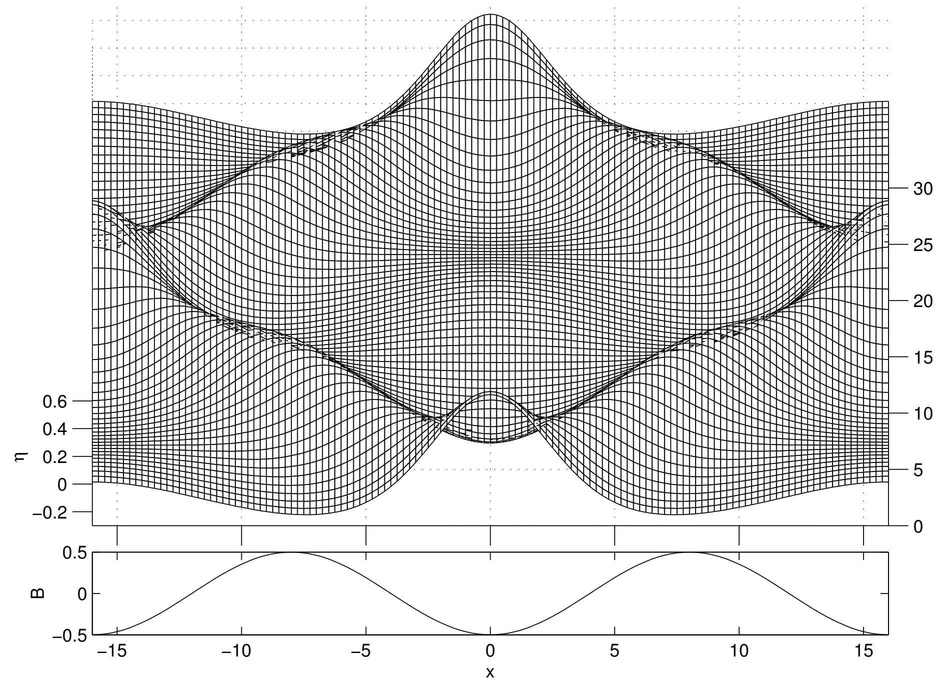

Figure 18: Reconstruction of free surface evolution for the solution (iii) in Figure 14.

7 Three-dimensional fluid motion: oblique incident waves.

In this section we extend the idea and technique developed in Section 2 to the three-dimensional fluid motion. In particular, we focus on the study of propagation and reflection of obliquely incident long periodic wave trains over equally long simple periodic topography features such as parallel sandbars. We start from the isotropic Benney-Luke type equation for weakly nonlinear, weakly dispersive waves, and show that the evolution of incident and reflected waves are described by a coupled system of Korteweg-de Vries equations similar to those derived previously if the angle of incidence is sufficiently large.

The isotropic Benney-Luke type equation describing weakly nonlinear, weakly dispersive waves over small topography was given in (2.7). Again we focus on the case where the amplitude of the waves is on the same order of the amplitude of the topography and set $\epsilon = \delta$.

$$f_{tt} - \triangle f = \epsilon \left[-\frac{1}{6}\triangle^2 f + \frac{1}{2}\triangle f_{tt} - f_t \triangle f - |\nabla f|_t^2 - b\triangle f - \nabla b \cdot \nabla f \right]. \tag{7.40}$$

We seek a solution of (7.40) consisting of 2 waves of the form

$$f = f_1(\theta_1, \tau) + f_2(\theta_2, \tau) + \epsilon \phi^{(1)}(\theta_1, \theta_2) + O(\epsilon^2), \tag{7.41}$$

$$\theta_j = \mathbf{k}_j \cdot \mathbf{x} - t + \epsilon \psi_j(\mathbf{x}, t) + O(\epsilon^2), \qquad j = 1, 2, \qquad \tau = \epsilon t,$$

where

$$\mathbf{x} = (x, z), \qquad \mathbf{k}_j = (k_{jx}, k_{jz}), \qquad |\mathbf{k}_j| = 1, \qquad j = 1, 2.$$

The direction of each wave is denoted by the unit vector $\mathbf{k}_j$, and thus we are seeking a solution to (7.40) as a superposition of nonlinear waves traveling in different directions. In the absence of bottom variation, a discrete set of plane waves at large angles to each other satisfy KdV equations independently [8], with small phase shifts at the intersection of the crests (these are contained in the ψ_j). Here, we anticipate that cumulative effect of $O(1)$ reflection from the periodic bottom will give rise to a coupling between two waves in terms of convolution integrals. With these definitions, the triad relation is

$$\mathbf{k}_1 - \mathbf{k}_2 = \mathbf{k}_b.$$

Substituting (7.41) in (7.40) yields, at leading order

$$2(1-\mathbf{k}_1\cdot\mathbf{k}_2)\partial_{\theta_1\theta_2}(f_1+f_2)=0,$$

which is trivially satisfied. At $O(\epsilon)$, we obtain

$$2(1-\mathbf{k}_1\cdot\mathbf{k}_2)\partial_{\theta_1\theta_2}\phi^{(1)}=F^{(1)}, \tag{7.42}$$

where the forcing term is given by

$$\begin{aligned}F^{(1)}=&\,2(1-\mathbf{k}_1\cdot\mathbf{k}_2)[\partial_{\theta_1}((\partial_{\theta_2}\psi_1)(\partial_{\theta_1}f_1))+\partial_{\theta_2}((\partial_{\theta_1}\psi_2)(\partial_{\theta_2}f_2))]\\&+2\partial_{\theta_1\tau}f_1+2\partial_{\theta_2\tau}f_2+\frac{1}{3}\partial^4_{\theta_1}f_1+\frac{1}{3}\partial^4_{\theta_2}f_2\\&+3(\partial_{\theta_1}f_1)(\partial^2_{\theta_1}f_1)+3(\partial_{\theta_2}f_2)(\partial^2_{\theta_2}f_2)\\&+(1+2\mathbf{k}_1\cdot\mathbf{k}_2)[(\partial_{\theta_1}f_1)(\partial^2_{\theta_2}f_2)+(\partial_{\theta_2}f_2)(\partial^2_{\theta_1}f_1)]\\&-\partial_{\theta_1}(b\partial_{\theta_1}f_1)-\partial_{\theta_2}(b\partial_{\theta_2}f_2)\\&-\mathbf{k}_1\cdot\mathbf{k}_2[(\partial_{\theta_1}b)(\partial_{\theta_2}f_2)+(\partial_{\theta_2}b)(\partial_{\theta_1}f_1)].\end{aligned} \tag{7.43}$$

We integrate (7.42) and impose the solvability condition that $\phi^{(1)}$ remains bounded in θ_1,θ_2, resulting in a coupled system of KdV equations for $u_1=\partial_{\theta_1}f_1, u_2=\partial_{\theta_2}f_2$:

$$\partial_\tau u_1+\frac{3}{2}u_1\partial_{\theta_1}u_1+\frac{1}{6}\partial^3_{\theta_1}u_1=\frac{1}{2}\mathbf{k}_1\cdot\mathbf{k}_2\left\langle u_2\partial_{\theta_1}b\right\rangle, \tag{7.44}$$

$$\partial_\tau u_2+\frac{3}{2}u_2\partial_{\theta_2}u_2+\frac{1}{6}\partial^3_{\theta_2}u_2=\frac{1}{2}\mathbf{k}_1\cdot\mathbf{k}_2\left\langle u_1\partial_{\theta_2}b\right\rangle, \tag{7.45}$$

where $\langle\cdot\rangle$ is the convolution integral that extracts out the cumulative effect of reflection from the bottom by taking average of integrand over fast variable. That is,

$$\begin{aligned}\left\langle u_2\partial_{\theta_1}b\right\rangle(\theta_1,\tau)=&\frac{1}{2L}\int_{-L}^{L}u_2(\theta_2,\tau)\partial_{\theta_1}b(\theta_1,\theta_2)\,d\theta_2,\\ \left\langle u_1\partial_{\theta_2}b\right\rangle(\theta_2,\tau)=&\frac{1}{2L}\int_{-L}^{L}u_1(\theta_1,\tau)\partial_{\theta_2}b(\theta_1,\theta_2)\,d\theta_1,\end{aligned}$$

where L is the common period of functions. Here u_j is proportional to the horizontal velocity of the fluid and the free surface displacement. Observe that the coupling between two waves due to reflection from topography is strongest when the waves are normally incident to and reflected from the horizontal topography features as in previous sections. Equations (7.44), (7.45) can easily be transformed to (2.19), (2.20) upon suitable scalings and integration by parts, noticing that one can write the resonant part of the topography as $b(\theta_1-\theta_2)$.

The equation (7.42) for $\phi^{(1)}$ can now be solved

$$\begin{aligned}\phi^{(1)}=&-[\psi_1u_1+\psi_2u_2]+\frac{(1+2\mathbf{k}_1\cdot\mathbf{k}_2)}{2(1-\mathbf{k}_1\cdot\mathbf{k}_2)}[f_1u_2+f_2u_1]\\&-\frac{1}{2(1-\mathbf{k}_1\cdot\mathbf{k}_2)}\left[u_1\int b\,d\theta_2+u_2\int b\,d\theta_1\right]\\&-\frac{\mathbf{k}_1\cdot\mathbf{k}_2}{2(1-\mathbf{k}_1\cdot\mathbf{k}_2)}\left[\int\widetilde{bu_2}\,d\theta_2+\int\widetilde{bu_1}\,d\theta_1\right],\end{aligned} \tag{7.46}$$

where $\tilde{f}$ is defined by $f-\langle f\rangle$. One can see from (7.46) that the original asymptotic expansion breaks down if $1-\mathbf{k}_1\cdot\mathbf{k}_2=O(\epsilon)$, that is, the angle between the wavevectors is $O(\epsilon^{1/2})$. In that case, a different expansion must be introduced to describe strong interaction between waves themselves. For the case of a flat bottom, the Kadomtsev-Petviashvili II (KP) equation is the appropriate asymptotic model. For a resonant topography, $|\mathbf{k}_b|=O(\epsilon^{1/2})$ and the evolution over resonant topography would probably require a variable-coefficient KP equation.

The solution (7.46) can also be used to determine the phase shifts ψ_j following the approach of [14, 11]. Physically, this represents extracting terms that preserve the memory of solitary collisions and speed fluctuations due to the bottom.

8 Conclusion

We have studied the evolution of long, periodic, waves over periodic topography whose length scale is comparable to that of the waves. The mechanism for interaction is Bragg scattering among two gravity waves and a Fourier component of the topography. Understanding cumulative action of these resonances can be an important part of describing the evolution of the wave spectrum near shallow water.

When cumulative effects of nonlinearity, dispersion, and repeated scattering become comparable the asymptotic behavior for long times is governed by coupled Korteweg-de Vries equations, the bottom serving as a catalyst for the energy exchange between the right- and left-traveling waves. Numerical simulations of these equations demonstrate this mechanism. We show that these systems conserve mass, total momentum and energy.

The main difference between this work and previous linear theories (for example, compare with [3, 4]) is in capturing the effect of nonlinearity in addition to the Bragg triad resonance, which allows us to obtain the long time evolution of the problem. These nonlinearities transfer energy into and out of wave-topography triads, an effect that is not present in previous theories. Previous weakly nonlinear theories (such as Benilov [9]) do not consider strong reflections.

There are extensions and applications in other fluid problems where a similar asymptotic framework is directly applicable. In stratified flows, three long internal wave modes can form a resonant triad and the asymptotic behavior in physical space would be described by three KdV equations coupled similarly to those derived in this study. The effect of uneven bottom configurations in the study of long wave generation in a horizontally oscillated water tank of finite length (Cox and Mortel [15]) can also be investigated in this framework.

9 Appendix A: Derivation of conserved quantities

We outline the proofs of the three conservation laws (3.25), (3.26), and (3.27). Retaining the convolution integrals in conservation form before the integration by parts is performed, we recast the equations (2.19), (2.20) as

$$u_\tau + uu_\xi + u_{\xi\xi\xi} = \langle (bv)_\zeta \rangle \,, \tag{9.47}$$

$$v_\tau - vv_\zeta - v_{\zeta\zeta\zeta} = -\langle (bu)_\xi \rangle \,. \tag{9.48}$$

Integrating (9.47), (9.48) with respect to ξ, ζ respectively from $-L$ to L, and using the periodicity of the functions, we easily conclude the mass conservation (3.25).

We multiply u to (9.47) and integrate with respect to ξ to obtain

$$\frac{d}{d\tau}\int_{-L}^{L} \frac{1}{2}u^2 \, d\xi = \frac{1}{2}\left\langle \int_{-L}^{L} u_\xi (bv)\, d\xi \right\rangle, \tag{9.49}$$

by changing the order of integration and using $u(bv)_\xi = (ubv)_\xi - u_\xi(bv)$. Similarly for v we obtain

$$\frac{d}{d\tau}\int_{-L}^{L} \frac{1}{2}v^2 \, d\zeta = -\frac{1}{2}\left\langle \int_{-L}^{L} v_\zeta (bu)\, d\zeta \right\rangle. \tag{9.50}$$

By using change of variables and integration by part, we find that

$$\left\langle \int_{-L}^{L} u_\xi (bv)\, d\xi \right\rangle = \left\langle \int_{-L}^{L} v_\zeta (bu)\, d\zeta \right\rangle. \tag{9.51}$$

Adding (9.49) and (9.50), we prove the conservation of momentum (3.26).

We multiply $u^2 + 2u_{\xi\xi}$ to (9.47) and integrate with respect to ξ to compute

$$\begin{aligned}\frac{d}{d\tau}\int_{-L}^{L}\left(\frac{1}{3}u^3 - u_\xi^2\right)\,d\xi &= -\left\langle \int_{-L}^{L}(u^2+2u_{\xi\xi})(bv)_\xi\,d\xi\right\rangle,\\ &= 2\left\langle \int_{-L}^{L}(uu_\xi + u_{\xi\xi\xi})(bv)\,d\xi\right\rangle,\\ &= -2\left\langle \int_{-L}^{L}(u_\tau + \langle (bv)_\xi\rangle)(bv)\,d\xi\right\rangle,\\ &= -2\left\langle \int_{-L}^{L}u_\tau vb\,d\xi\right\rangle,\end{aligned} \tag{9.52}$$

where (9.47) is used in the third equality. Similar manipulations applied to v results in

$$\frac{d}{d\tau}\int_{-L}^{L}\left(\frac{1}{3}v^3 - v_\zeta^2\right)\,d\zeta = -2\left\langle \int_{-L}^{L}v_\tau ub\,d\zeta\right\rangle. \tag{9.53}$$

Adding (9.52) and (9.53) yields the nonlocal conservation of energy (3.27).

10 Acknowledgements

Partial support for Paul Milewski from NSF-DMS is gratefully acknowledged.

References

[1] Hasselmann, K., Feynman diagrams and interaction rules of wave-wave scattering processes. *Rev. Geophys. Space Phys.*, **4**, pp. 1–32 (1966)

[2] Long, R. B., Scattering of surface waves by an irregular bottom. *J. Geophys. Res.*, **78**, pp. 7861–7870 (1973)

[3] Davies, A. G., Heathershaw, A. D., Surface-wave propagation over sinusoidally varying topography. *J. Fluid Mech.*, **144**, pp. 419–443 (1984)

[4] Mei, C. C., Resonant reflection of surface water waves by periodic sandbars. *J. Fluid Mech.*, **152**, pp. 315–335 (1985)

[5] Lelong, M., Riley, J. J., Internal wave-vortical mode interactions in strongly stratified flows. *J. Fluid Mech.*, **232**, pp. 1–19 (1991)

[6] Milewski, P. A., Benney, D. J., Resonant interactions between vortical flows and water waves. Part I: Deep water. *Stud. in Appl. Math.*, **94**, pp. 131–167 (1995)

[7] Milewski, P. A., Resonant interactions between vortical flows and water waves. Part II: Shallow water. *Stud. in Appl. Math.*, **94**, pp. 225–256 (1995)

[8] Benney, D. J., Luke, J. C.. On the interactions of permanent waves of finite amplitude. *J. Math. Phys.*, **43**, pp. 309–313 (1964)

[9] Benilov, E. S., On the surface waves in a shallow channel with an uneven bottom. *Stud. in Appl. Math.*, **87**, pp. 1–14 (1992)

[10] Newell, A. C., Solitons in Mathematics and Physics. vol. 48 of CBMS, SIAM, 1974

[11] Milewski, P. A., Long wave interaction over varying topography. *Physica D*, **123**, pp. 36–47 (1998)

[12] Grimshaw, R., Tian, X. Periodic and chaotic behaviour in a reduction of the perturbed Korteweg-de Vries equation. *Proc. Roy. Soc. London Ser. A*, **445**, no. 1923, 1–21 (1994).

[13] Milewski, P. A., Tabak, E. G., A pseudospectral procedure for the solution of nonlinear wave equations with examples from free-surface flows. *SIAM J. Sci. Comput.*, **21**, 1102–1114 (1999).

[14] Su, C. A., Mirie, R. M., On head-on collisions between two solitary waves. *J. Fluid Mech.*, **98**, pp. 509–525 (1980)

[15] Cox, E. A., Mortell, M. P. The evolution of resonant water-wave oscillations. *J. Fluid. Mech.*, **162**, pp. 99–116 (1986)